BRAIN COMMUNICATIONS

Neuron-autonomous susceptibility to induced synuclein aggregation is exacerbated by endogenous *Lrrk2* mutations and ameliorated by *Lrrk2* genetic knock-out

Sarah MacIsaac,[1] Thaiany Quevedo Melo,[2,*] Yuting Zhang,[2,*] Mattia Volta,[1,3] Matthew J. Farrer[1,4] and Austen J. Milnerwood[1,2]

*These authors contributed equally to this work.

Neuronal aggregates containing α-synuclein are a pathological hallmark of several degenerative diseases; including Parkinson's disease, Parkinson's disease with dementia and dementia with Lewy bodies. Understanding the process of α-synuclein aggregation, and discovering means of preventing it, may help guide therapeutic strategy and drug design. Recent advances provide tools to induce α-synuclein aggregation in neuronal cultures. Application of exogenous pre-formed fibrillar α-synuclein induces pathological phosphorylation and accumulation of endogenous α-synuclein, typical of that seen in disease. Genomic variability and mutations in α-synuclein and leucine-rich repeat kinase 2 proteins are the major genetic risk factors for Parkinson's disease. Reports demonstrate fibril-induced α-synuclein aggregation is increased in cells from leucine-rich repeat kinase 2 pathogenic mutant (G2019S) overexpressing mice, and variously decreased by leucine-rich repeat kinase 2 inhibitors. Elsewhere *in vivo* antisense knock-down of leucine-rich repeat kinase 2 protein has been shown to protect mice from fibril-induced α-synuclein aggregation, whereas kinase inhibition did not. To help bring clarity to this issue, we took a purely genetic approach in a standardized neuron-enriched culture, lacking glia. We compared fibril treatment of leucine-rich repeat kinase 2 germ-line knock-out, and G2019S germ-line knock-in, mouse cortical neuron cultures with those from littermates. We found leucine-rich repeat kinase 2 knock-out neurons are resistant to α-synuclein aggregation, which predominantly forms within axons, and may cause axonal fragmentation. Conversely, leucine-rich repeat kinase 2 knock-in neurons are more vulnerable to fibril-induced α-synuclein accumulation. Protection and resistance correlated with basal increases in a lysosome marker in knock-out, and an autophagy marker in knock-in cultures. The data add to a growing number of studies that argue leucine-rich repeat kinase 2 silencing, and potentially kinase inhibition, may be a useful therapeutic strategy against synucleinopathy.

1 Department of Human Genetics, Centre for Applied Neurogenetics, University of British Columbia, Vancouver, BC, Canada
2 Department of Neurology and Neurosurgery, Montreal Neurological Institute, McGill University, Montreal, QC, Canada
3 EURAC Research, Institute for Biomedicine, Bolzano, Italy
4 Department of Neurology, University of Florida, Gainesville, FL, USA

Correspondence to: Austen J. Milnerwood, Department of Neurology and Neurosurgery,
Montreal Neurological Institute, McGill University, Montreal, QC, Canada
E-mail: austen.milnerwood@mcgill.ca

Keywords: LRRK2; alpha-synuclein; aggregation; Parkinson's disease, axon

Received September 16, 2019. Revised December 4, 2019. Accepted December 5, 2019. Advance Access publication January 7, 2020

Abbreviations: AAV = adeno-associated virus; ACB = aggregate-containing cell body; aSyn = α-synuclein; BAC = bacterial artificial chromosome; DAPI = 4′,6-diamidino-2-phenylindole; DMSO = dimethyl sulfoxide; DIV = days *in vitro*; GFP = green fluorescent protein; GKI = G2019S knock-in; KO = knock-out; LAMP1 = Lysosomal-associated membrane protein 1; LDH = lactate dehydrogenase; LKO = LRRK2 knock-out; LRRK2 = leucine-rich repeat kinase 2; MAP2 = microtubule-associated protein 2; p62 = ubiquitin-binding protein p62; PBS = phosphate-buffered saline; PFF = pre-formed fibrillar aSyn; pS129 = phosphorylated serine 129 (on aSyn); WT = wild-type

Graphical Abstract

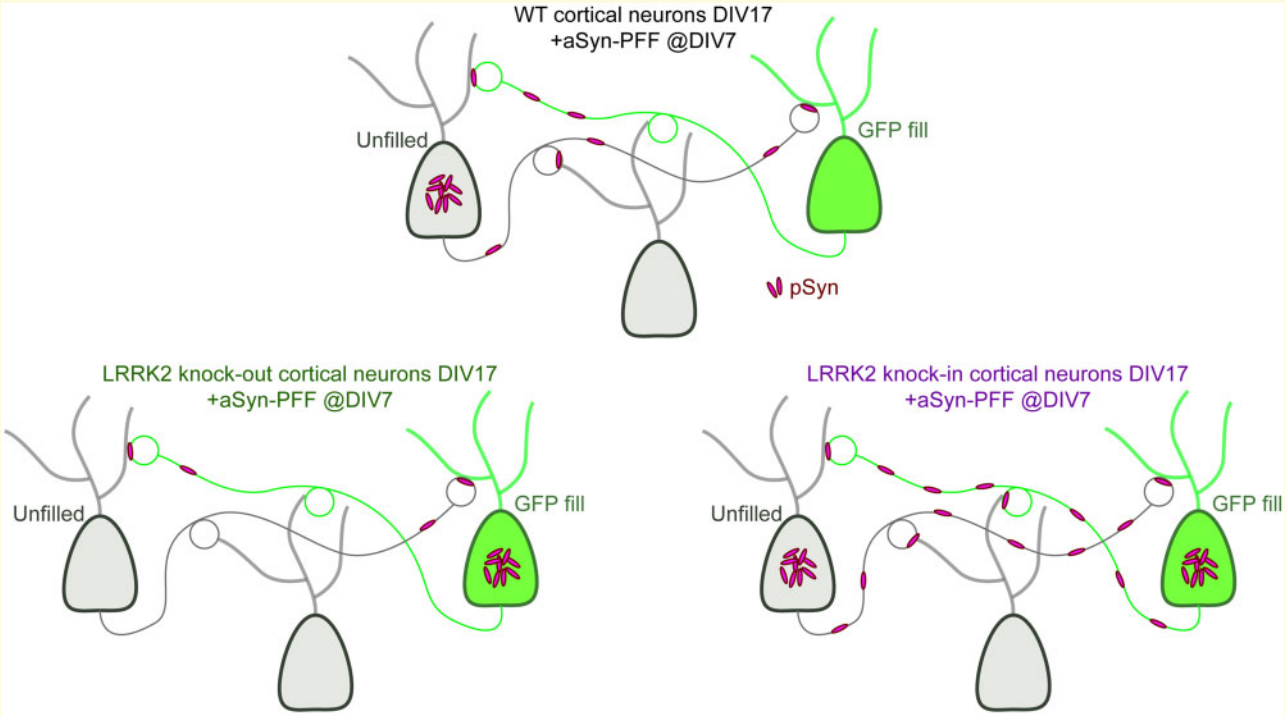

Introduction

Although exactly how and why they form is currently unknown, neuronal inclusions containing the synaptic protein α-synuclein (aSyn), termed Lewy bodies and Lewy neurites, are a pathological hallmark of several degenerative diseases (reviewed in Goedert *et al.*, 2013). Parkinson's disease has Lewy pathology by definition, as do Parkinson's disease with dementia and dementia with Lewy bodies.

In late-stage Parkinson's disease, post-mortem Lewy pathology is observed in surviving nigral cells, but also throughout the brain, to varying degrees (reviewed in Goedert *et al.*, 2013; Giguère *et al.*, 2018). Toxic aSyn is proposed to spread, seeding pathology like a prion (Brundin and Melki, 2017), although this is hotly debated (Surmeier *et al.*, 2017). aSyn is secreted by exocytosis, a process that is dependent upon synaptic activity (Lee *et al.*, 2005; Paillusson *et al.*, 2013) and while there is little, if any, aSyn in dopamine axons, it is heavily enriched in cortico-striatal terminals (Emmanouilidou *et al.*, 2016; Taguchi *et al.*, 2016). Thus, aSyn may pass from cortical terminals to the extracellular matrix, and then into other nearby axons, such as nigrostriatal axons in Parkinson's disease (reviewed in Foffani and Obeso, 2018).

Genomic variability and mutations in the genes *SNCA* (coding aSyn) and *Lrrk2* (coding LRRK2) are the major genetic risk factors for Parkinson's disease (reviewed in Volta *et al.*, 2015). Synuclein duplications and triplications are pathogenic, whereas pathogenic LRRK2 mutations (the most common being G2019S) increase LRRK2 kinase activity, suggesting a gain of function in both scenarios. A synergistic pathogenesis was demonstrated by accelerated pathology in aSyn overexpressing mice when crossed to LRRK2 overexpressing mice [both wild-type (WT) LRRK2 and G2019S mutant], and conversely pathology was attenuated when they were crossed with LRRK2 knock-out (LKO) mice (Lin *et al.*, 2009). Similarly, viral expression of aSyn worsens pathology in LRRK2 overexpressing rats (Daher *et al.*, 2015), whereas LKO rats are protected (Daher *et al.*, 2014). Although two other studies failed to reproduce a clear pathological synergy between LRRK2 and aSyn overexpression (Daher

et al., 2012; Herzig *et al.*, 2012), possibly due to ceiling effects or transgene expression patterns, the weight of evidence shows LKO to be protective against synuclein overexpression (reviewed in Cresto *et al.*, 2019).

Exogenous pre-formed fibrillar aSyn (PFF) exposure induces pathological phosphorylation (pS129) and accumulation of endogenous aSyn, typical of Lewy pathology; this has been demonstrated in cell lines (Luk *et al.*, 2009), neurons (Volpicelli-Daley *et al.*, 2011), aSyn overexpressing mice (Luk *et al.*, 2012*b*), WT mice (Luk *et al.*, 2012*a*) and rats (Paumier *et al.*, 2015). This approach enables control over the amount of aSyn used to induce pathology, and has been used to examine the contribution of LRRK2 to aSyn pathology. In hippocampal primary neuron cultures, the aggregation of pS129 aSyn is increased by ~25% in cells from LRRK2 G2019S mutant BAC overexpressing mice (Volpicelli-Daley *et al.*, 2016; Henderson *et al.*, 2018). These studies also demonstrated protective effects of LRRK2 kinase inhibition, although one study observed reduced pS129 aggregation in WT and LRRK2 overexpressing cells (Volpicelli-Daley *et al.*, 2016), whereas only mutant increases were reduced in the other (Henderson *et al.*, 2018). Reports using *in vivo* approaches demonstrated antisense knock-down of LRRK2 protein protected mice from PFF-induced pSer129 aggregation (Zhao *et al.*, 2017), but kinase inhibition did not (Henderson *et al.*, 2019). This raises the possibility that non-kinase functions of LRRK2 are protective *in vivo*.

LRRK2 is expressed in many tissues and levels are high in peripheral monocytes (Thévenet *et al.*, 2011). Furthermore, immune responses in the brain are elevated in LRRK2 BAC mutant overexpressing mice (Kozina *et al.*, 2018) and deadened in LKO mice (Puccini *et al.*, 2015), raising the possibility that LRRK2 effects on aSyn aggregation are through non-neuronal cells.

In an attempt to bring more clarity to the issue, we aimed to determine whether LRRK2 mutations exacerbate, and LRRK2 genetic knock-out protects against, aSyn aggregation specifically in neurons. Using a genetically faithful LRRK2 G2019S knock-in (GKI) model, in direct comparison to a germ-line LKO, we found primary neuron cortical cultures, entirely lacking astrocytes and microglia, develop pS129 aggregates predominantly within axonal processes. Moreover, we observed that LKO mice are protected from PFF-induced pS129 accumulation, whereas those from GKI mice are more sensitive. Protection and vulnerability correlated with basal increases in markers of lysosome function (LAMP1) and impaired autophagy (p62), respectively.

Materials and Methods

Genetic models and neuronal culture

C57Bl/6J WT, LKO and GKI mice (Beccano-Kelly *et al.*, 2014, 2015; Volta *et al.*, 2017) were maintained according to the Canadian Council on Animal Care regulations. Primary cortical neuron cultures were prepared from homozygous LKO, homozygous LRRK2 GKI, and WT littermate embryos, plated and maintained as previously (Beccano-Kelly *et al.*, 2014; Munsie *et al.*, 2014). In brief, brains were dissected at E16.5–17.5 and placed in 1 ml Hibernate-E medium supplemented with B-27 on ice while tail samples were genotyped by PCR prior to pooling by genotype. Cortices were micro-dissected in Hank's Balanced Salt Solution supplemented with 0.03% D-glucose, 0.01% HEPES, 0.01% penicillin/streptomycin (HBSS+) and trypsin digested (0.05% Trypsin-0.25% EDTA) for 10 min at 37°C. Following addition of trypsin inhibitor, cells were centrifuged and re-suspended with neurobasal medium supplemented with 0.02% B-27 and 0.0025% L-glutamine (NBM+) and DNase I. Tissue was thoroughly triturated and re-centrifuged before neurons were counted and seeded at 250 000 cells/well in 1 ml NBM+ on poly-D-lysine coated cover slips in 24-well plates.

To visualize neuronal architecture in individual neurons, cultures were nucleofected prior to plating; following cell counts, neurons were pelleted by light centrifugation, re-suspended in electroporation buffer (Mirus) with 1 μg pAAV-GFP-CAG plasmid (Adgene)/million cells and electroporated (Amaxa Nucleofector2b, Lonza). Nucleofected cells were mixed 50:50 in NBM+ with non-nucleofected cortical neurons from the original source and plated at 250 000 cells/well. All cultures were maintained at 37°C in a humidified incubator with 5% CO_2. After DIV4, an additional 10% of media was added to each well every 4–5 days.

PFF and treatment

Batches of recombinant aSyn PFFs were obtained following quality control by sedimentation, electron microscopy, thioflavin T and endotoxin assays, from the laboratory of Dr. Laura Volpicelli-Daley (University of Alabama, Birmingham) and in-house, PFFs were examined by transmission electron microscopy to confirm the initial integrity of PFF fibrillar ultrastructure, and effective breakdown to oligomeric seed structures following sonication (Supplementary Fig. 1), according to standard protocols (Volpicelli-Daley *et al.*, 2011, 2014*b*, 2016). Immediately prior to treatment of cortical cultures at div7, PFFs were diluted in phosphate-buffered saline (PBS) and subject to probe tip sonication (Dismembrator 120; Fischer Scientific; 30 s of 1 s on/off pulses, 50% max intensity). Culture treatment was performed by adding 0.5 ml of media from each well to a 15-ml Falcon tube, adding PBS, aSyn monomer or PFFs to a final concentration of 2 μg/ml, mixing and replacing media to each well to give a final concentration of 1 μg/ml. After a single PFF application, cells were maintained as detailed in the neuronal culture section above for 10 days (to div17).

Lactate dehydrogenase cell death assay

Cell integrity was assessed by lactate dehydrogenase (LDH)-based colorimetric assay (Sigma) at div9, 12 and 17 as per manufacturer's instructions. Media from each condition were pooled into separate Eppendorf tubes. Positive (media from a well exposed to 8% TritonX-100) and negative (media) controls were included. Tubes underwent brief centrifugation to sediment cell debris, supernatant was removed, mixed thoroughly with 1:1:1 with NAD+ substrate, reduction co-factor and NADH-interacting probe (max absorption wavelength = 450nm). Solution from each condition was added to 96-well plates in triplicate and left to incubate for 30 min. A microplate reader detected the optical density of each well. Condition triplicates were averaged and the serum-free media value was subtracted in each condition to examine membrane integrity as a readout of toxicity, relative to positive controls (100% cell death; Triton X).

Immunocytochemistry and fluorescence microscopy

At div17, neurons were fixed in 4% paraformaldehyde (PFA in 4% sucrose) for 15 min, followed by 3× 10 min PBS washes and blocked for 1 h in 5% normal goat serum (NGS; Gibco, 16210-072 in PBS). Primary antibodies were diluted in an antibody solution of 2% NGS in PBST (0.2% Tween-20). After overnight incubation at 4°C, neurons were washed and blocked for 1 h. Secondary antibodies (Alexa-488 and Alexa-568 conjugated rabbit and mouse, Molecular Probes) were diluted in antibody solution (1:1000) and incubated (dark 30 min) followed by 3 × 10 min PBS washes. Coverslips were mounted with fluoromount (Southern Biotech). Primary antibodies included: rabbit anti-GFP (1:1000; Abcam, ab6556), chicken anti-GFP (1:1000; Abcam, ab13970), rabbit anti-GFAP (1:1000; Abcam, ab7260), goat anti-Iba1 (1:1000; Novus Biologicals, NB100-1028), rabbit anti-p62 (1:500; Abcam, ab91526), rabbit anti-LAMP1 (1:250; Abcam, ab24170), rabbit aSyn (1/200: Cell Signaling, 4179) and mouse anti-pS129 aSyn (1:1000; Abcam, ab184674).

Images for DAPI and field pS129 aSyn quantification were obtained with an EVOS FL Auto Imaging System and acquired at 40×. Images taken for field p62 and LAMP1 quantification, cell body stain quantification and co-localization, were obtained with an Olympus Fluoview 1000 confocal microscope and acquired as 1um z-stacks at 60×. For DAPI quantification, images were binarized using ImageJ and a CellProfiler pipeline designed to recognize circular objects was used to count nuclei. Manual scoring was used to count pyknotic, condensed or fragmented nuclei (herein pyknotic). For field stain quantification, images were batch thresholded blind, using Photoshop (Adobe), and mean grey values for each image quantified with ImageJ. Values were normalized to average density of healthy nuclei within that condition. Affected cell bodies (containing somatic pS129 aSyn signal) were counted manually in each condition and normalized to the average density of healthy nuclei. Affected cell bodies were masked out of all images for neuritic p-syn quantification, subsequently performed as 'field quantification'. For cell body quantification, pS129 aSyn, p62 and LAMP1 stained images were batch thresholded, blind, using Photoshop, regions of interest were drawn by hand in ImageJ and mean grey values were quantified. For co-localization, images, Pearson's R coefficient was calculated with ImageJ. All acquisition and analysis parameters were constrained within each culture.

Data reporting and statistical analyses

Data were collated and tested in Graphpad Prism 8 and presented as mean ± standard error of the mean, overlaid on scatter plots or bar-paired scatter plots. Experimental n is culture or image field from (n) cultures. Pairwise comparisons were by unpaired two-tailed Student's t-test (Figs 1B and 5D and G), or paired two-tailed Student's T-test on raw values (Figs 3 and 4D–F, with F normalized for clarity). LDH toxicity and pyknosis grouped data were analysed by one-way RM-ANOVA (Figs 3B and 4B). aSyn staining was analysed by one-way ANOVA, with the appropriate *post-test*, as detailed in the text (Figs 3C and 4C) or Welch-corrected one-way ANOVA (unequal standard deviation, Fig. 5B, C, E and F) and *post hoc* comparisons corrected by False Discovery Rate using the two-stage step-up method of Bejamini, Krieger and Yekutieli (Fig. 5B and E).

Data availability

Data are available on direct request to the corresponding author.

Results

PFF, but not monomeric, aSyn induces axonal and somatic pS129 aSyn accumulation

Primary neuronal cultures of mouse cortex were maintained to DIV17, following treatment with either PBS vehicle control, monomeric aSyn or PFF, for 10 days. Immunostaining for mouse aSyn in untreated or PBS-treated neurons reveals weak nuclear staining and bright punctate signal (Fig. 1A), typical of neuronal aSyn in axon terminals, where synuclein is enriched (Murphy *et al.*, 2000; Froula *et al.*, 2018). In cultures treated with PFF, aSyn staining revealed the same typical punctate

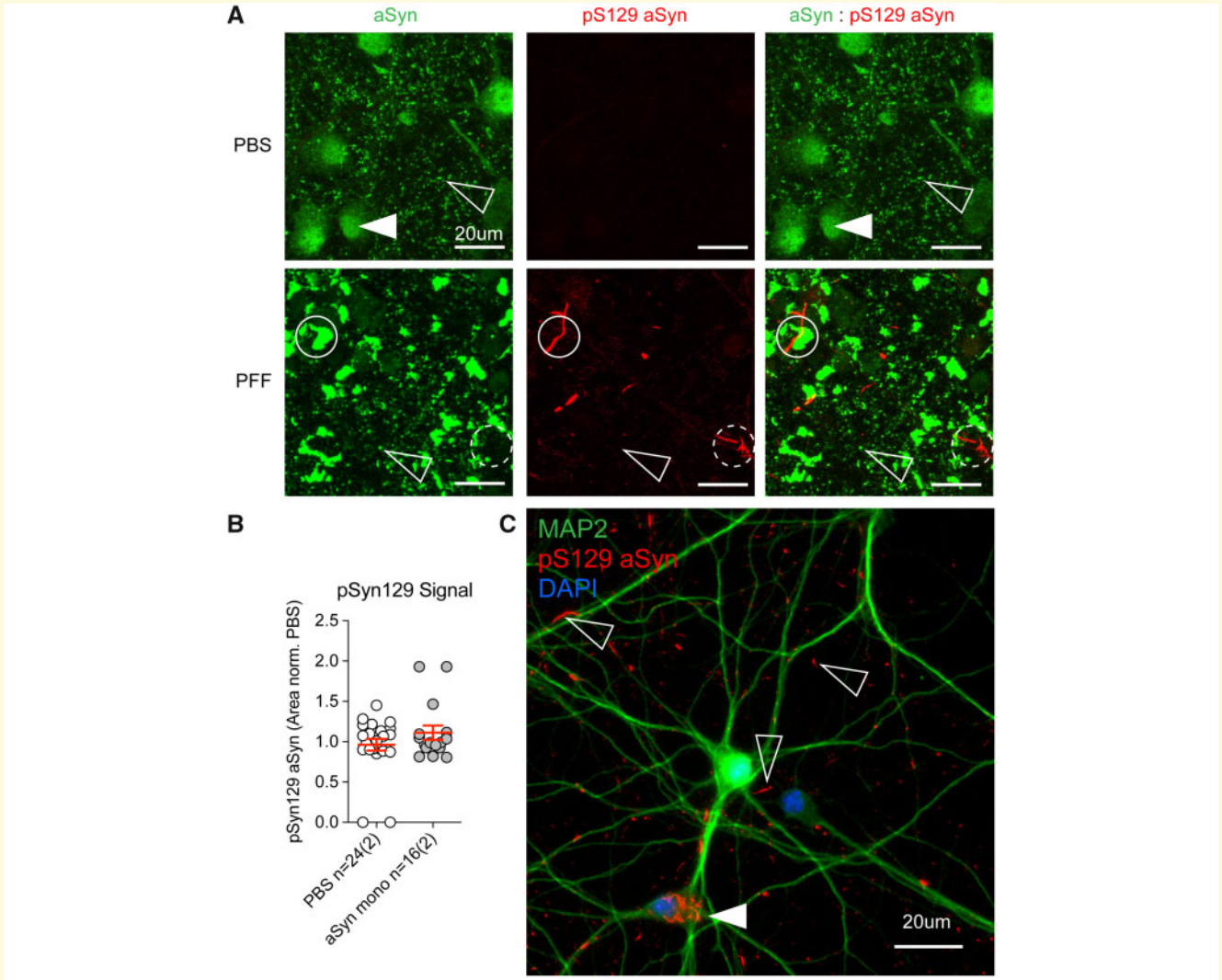

Figure 1 Application of aSyn pre-formed fibrils, but not monomeric aSyn, induces phosphorylated aSyn aggregate formation in neuronal cultures. (**A**) Representative example immunofluorescent confocal microscopy images of mouse primary cortical neurons at 17-days *in vitro* (div17), 10 days following application of saline control (PBS) or aSyn pre-formed fibrils (PFF). Cultures were stained for aSyn (aSyn; green) and pathologically phosphorylated aSyn (pS129 aSyn; red). In PBS-treated cultures, endogenous aSyn staining (green) is observed as diffuse nuclear signal (closed arrowhead) and punctate staining of aSyn throughout the neuropil, typical of that seen in axon terminals (open arrowhead). Only weak background pS129 aSyn signal is observed and no distinct structures. In PFF-treated cultures, aSyn staining reveals large clumps of exogenous fibrillar aSyn (open circle) in addition to typical endogenous aSyn puncta (open arrowhead). Red pS129 aSyn staining reveals large serpentine aggregates (passing through open circle), complex aggregates (dashed circle) and puncta throughout the neuropil; there is little overlap with the large fibrillar aSyn clumps (green) and little co-localization between pS129 aSyn and aSyn signal. (**B**) Quantification of pS129 aSyn signal in div17 cortical cultures treated at div7 with the same concentration of non-fibrillar monomeric aSyn; there is no pS129 aSyn signal above background, as observed in PBS-treated cultures (Student's *t*-test, $P = 0.2$; $n = 24$ and 16 image fields, from two independent cultures). (**C**) Representative example immunofluorescent microscopy image of div17 PFF-treated culture stained for the neuronal dendritic marker microtubule-associated protein 2 (MAP2, green), nuclei (DAPI, blue) and pS129 aSyn (red). In these neuronally enriched cultures at div21, nuclei are within MAP2-stained soma. Serpentine pS129 aSyn stain is seen throughout the image field, but is predominantly not associated with dendritic MAP2 (open arrowheads). Occasional soma is seen to contain large, complex, pS129 aSyn aggregates (closed arrowhead).

pattern, with additional large extracellular clumps, reflecting the presence of exogenous aSyn PFF.

When aSyn is recruited into inclusions characteristic of Lewy Pathology, it undergoes phosphorylation at Ser129 (pS129), thus antibodies against pS129 selectively stain pathological inclusions (Fujiwara *et al.*, 2002; Volpicelli-Daley *et al.*, 2011). As shown in Fig. 1A, pS129 aSyn staining revealed punctate and serpentine structures, specifically in PFF-treated cultures, in agreement with previous studies (Volpicelli-Daley *et al.*, 2011, 2014*a*, 2016). As expected, pS129 aSyn staining in PFF-treated cultures did not detect clumps of fibrillar aSyn; as this

modification is absent in recombinant aSyn and the accumulation of pS129 aSyn reflects intracellular modification of endogenous aSyn. Treatment with the same concentration of monomeric aSyn did not induce pS129 aSyn accumulation, as demonstrated by no increase in pS129 aSyn signal above background levels in PBS-treated cultures (Fig. 1B).

To examine the subcellular localization of pS129 aSyn aggregates, cultures were co-stained with a nuclear dye (DAPI) and the neuronal somato-dendritic marker, MAP2 (Fig. 1C). The vast majority of pS129 aSyn staining, apparent throughout the cultures, did not associate with MAP2 staining of dendrites, and appeared to be within structures that opposed or passed over neuronal dendritic processes, presumably in axonal compartments. A small percentage of cells exhibited pronounced somatic pS129 aSyn staining, which was excluded from the nucleus (Fig. 1C), herein termed Aggregate Cell Bodies (ACBs). To confirm that non-somatic pS129 aSyn accumulation was within axons, cells were nucleofected with AAV-GFP (at day of plating) and mixed with non-nucleofected cells; this provides a low percentage of neurons containing a GFP fill (10–30%), in which axons and fine dendritic processes such as spines and filopodia can be visualized. Cultures containing GFP-filled cells were treated with the same paradigm, prior to DAPI and immunofluorescence staining against nuclei, pS129 aSyn and GFP (Fig. 2). As exemplified in Fig. 2A, pS129 aSyn inclusions are apparent in the axon of cells at varicosities within 100 µm of the soma. In axon terminal fields, several hundred microns from the soma, a high density of inclusions are observed, many in large blebs, and many associated with apparently broken processes, indicative of degenerating axons (Fig. 2B). Axonal aggregates were observed in most GFP-filled cells, the vast majority of which do not exhibit somatic pS129 aSyn aggregates/ACBs.

Cultures from LKO mice are resistant to PFF-induced pS129 aSyn inclusion formation, which occurs without increased cellular toxicity

To investigate the potential role of LRRK2 in modulating aSyn pathology, we subjected cortical neuronal cultures from LKO and WT littermate cortices to PFF treatment (Fig. 3A). There was no increase in cellular toxicity produced by PFF treatment, as indicated by similar levels of LDH activity (~10% of positive control) in media from PBS- and PFF-treated cultures at div17 (Fig. 3B). A similar lack of LDH assay toxicity was observed at div9 and div12 (not shown). As a second measure of culture health, the percentage of pyknotic nuclei was counted in each condition (Fig. 3B); in agreement with results from the LDH assay, there was no increase in the proportion of unhealthy nuclei in PFF-treated cultures from either WT or LKO mice.

Immunocytochemical staining of pS129 aSyn, and quantification of signal area (relative to culture cell density), demonstrated a large increase in pS129 pSyn following PFF treatment of WT cultures. A similar increase was observed in PFF-treated LKO cultures, but this was significantly reduced at 45% of WT levels (Fig. 3C). To determine how many neurons contained somatic pS129 aSyn aggregates, and whether decreases in pathological aSyn levels in LKO cultures were due to alterations in these somatic aggregates, cell soma containing pS129 (ACBs) were quantified (Fig. 3D). On average ~4% of cells were classified as ACBs in WT PFF-treated neurons and, while there was a strong trend towards a reduced proportion of ACBs in sister cultures from LKO mice, there was no significant difference in the number of ACBs (Fig. 3D). Decreased pS129 aSyn signal in LKO cultures could be due to less pS129 aSyn signal within a similar proportion of ACBs. Quantification of pS129 aSyn signal within ACBs demonstrated no difference (and no trend) between WT and LKO in the levels of signal within ACBs (Fig. 3E). When analysis of pS129 aSyn signal was conducted in the absence of ACBs (masked out), to give neuritic pS129 aSyn staining, there was still a highly significant decrease in LKO cultures (Fig. 3F).

Together the data demonstrate that PFF treatment induces pS129 aSyn accumulation in the absence of (or prior to) cell death within 10 days in developing neuronal networks. Although PFFs induce pronounced pS129 aSyn aggregation in axonal compartments by 10 days' treatment, only a small percentage of neurons (~5%) have aggregates forming within their cell body. LKO sister cultures are resistant to PFF-induced pathological conversion of aSyn, exhibiting significantly less pS129 aSyn signal throughout their neuropil. While there is a strong trend towards fewer ACBs in LKO cultures, there is no difference in the amount of pS129 aSyn within the cell soma of those that do.

Cultures from LRRK2 GKI mice are more sensitive to PFF-induced pS129 aSyn inclusion formation

To test whether LRRK2 mutations that are causal to Parkinson's disease increase sensitivity of neurons to induced aSyn pathology, GKI and WT littermate cortical cultures were PFF-treated (Fig. 4A). As with WT neurons from LKO cultures, there was no increase in cellular toxicity produced by PFF treatment, as indicated by similar levels of LDH activity and the percentage of pyknotic nuclei in WT cultures (Fig. 4B). There was similarly no cellular toxicity produced by PFF treatment of GKI mouse cultures by either measure (Fig. 4B).

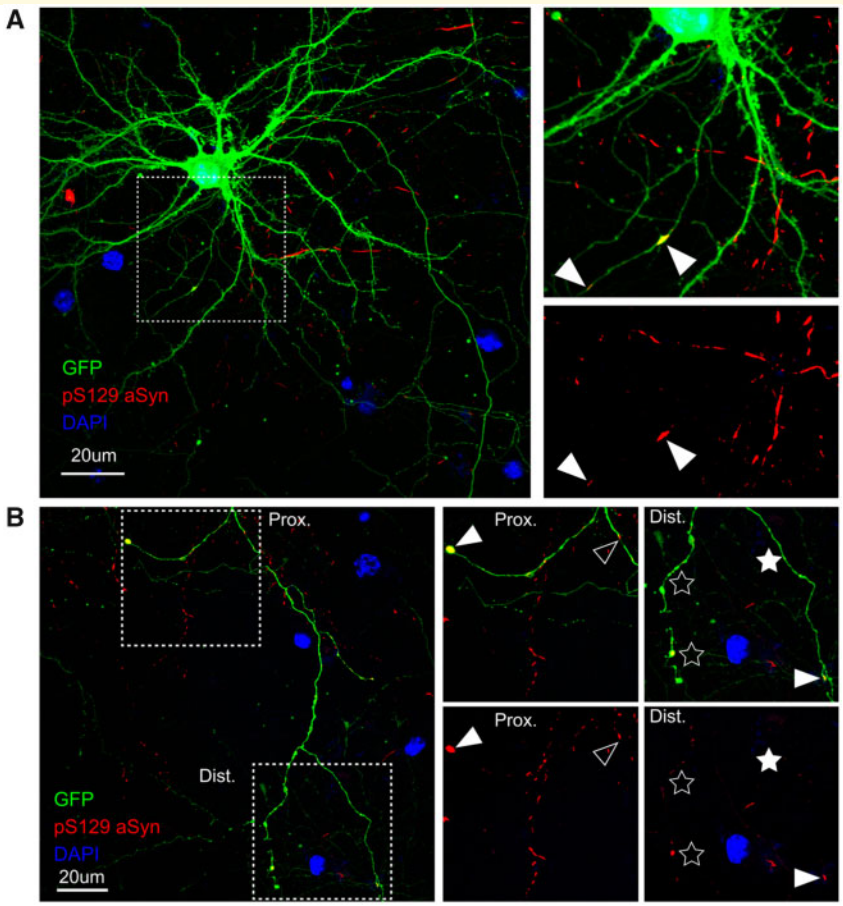

Figure 2 In the absence of somatic aggregation, pS129 aSyn accumulation is seen in degenerating axon segments. (**A**) Representative example (left) immunofluorescent confocal microscopy image of GFP expressing (anti-GFP; green) WT cortical neurons at div17, 10 days following application of PFF. Cultures were stained for nuclei (DAPI; blue) and pS129 aSyn (red). pS129 aSyn staining surrounds the neuron but is not present within somatic or dendritic compartments. Upon close examination (top right) of the area marked in left micrograph (dashed open rectangle), an axon varicosity is filled with pS129 signal, and a smaller accumulation is seen within a regular axonal segment (closed arrowheads). (**B**) The terminal region of an axon emanating from the same cell shown in A (~300 μm from soma). Two regions, proximal (Prox.) and more distal (Dist.) are delineated by dashed open rectangles and expanded to the right. In the proximal region, a large terminal varicosity contains pS129 aSyn (closed arrowhead), and pS129 aSyn accumulation is also seen within a regular axonal process (open arrowhead). In the distal segment, a terminal varicosity contains pS129 aSyn (closed arrowhead) and a regular process contains several small pS129 aSyn puncta (closed star). A second segment contains multiple swellings/varicosities and probable breakpoints that containing pS129 aSyn signal (open stars).

Immunocytochemical staining of pS129 aSyn, and quantification of signal area (relative to culture cell density), demonstrated a large increase in pS129 pSyn following PFF treatment of WT cultures (Fig. 4A and C; to an almost identical level as WT cultures in LKO experiments in Fig. 3C). A similar increase was observed in PFF-treated GKI cultures, but this was significantly increased to ~3-fold that of WT levels (Fig. 4C). To determine whether increases in pathological aSyn levels in GKI cultures were due to alterations in somatic aggregation, cell soma containing pS129 pSyn (ACBs) were quantified (Fig. 4D). On average ~5% of WT cells were classified as ACBs, and there was a significant increase in the proportion of ACBs in sister cultures from GKI mice (Fig. 4D). In GKI cultures, there was a strong but non-significant trend to increased pS129 aSyn signal within ACBs (Fig. 4E). When analysis of pS129 aSyn signal was conducted in the absence of ACBs, the levels of neuritic pS129 aSyn staining were significantly increased in GKI cultures (Fig. 4F).

Together the data again demonstrate that PFF treatment induces pS129 aSyn accumulation in the absence of (or prior to) cell death and that only a small percentage of neurons (~5%) have aggregates forming within their cell body in WT cells. The presence of the Parkinson's disease mutation in GKI sister cultures results in increased sensitivity to PFF-induced pathological aSyn conversion. GKI cultures exhibit significantly more pS129 aSyn signal throughout neuropil, with more cell bodies affected, and a trend towards increased pS129 aSyn within the cell soma of those that do.

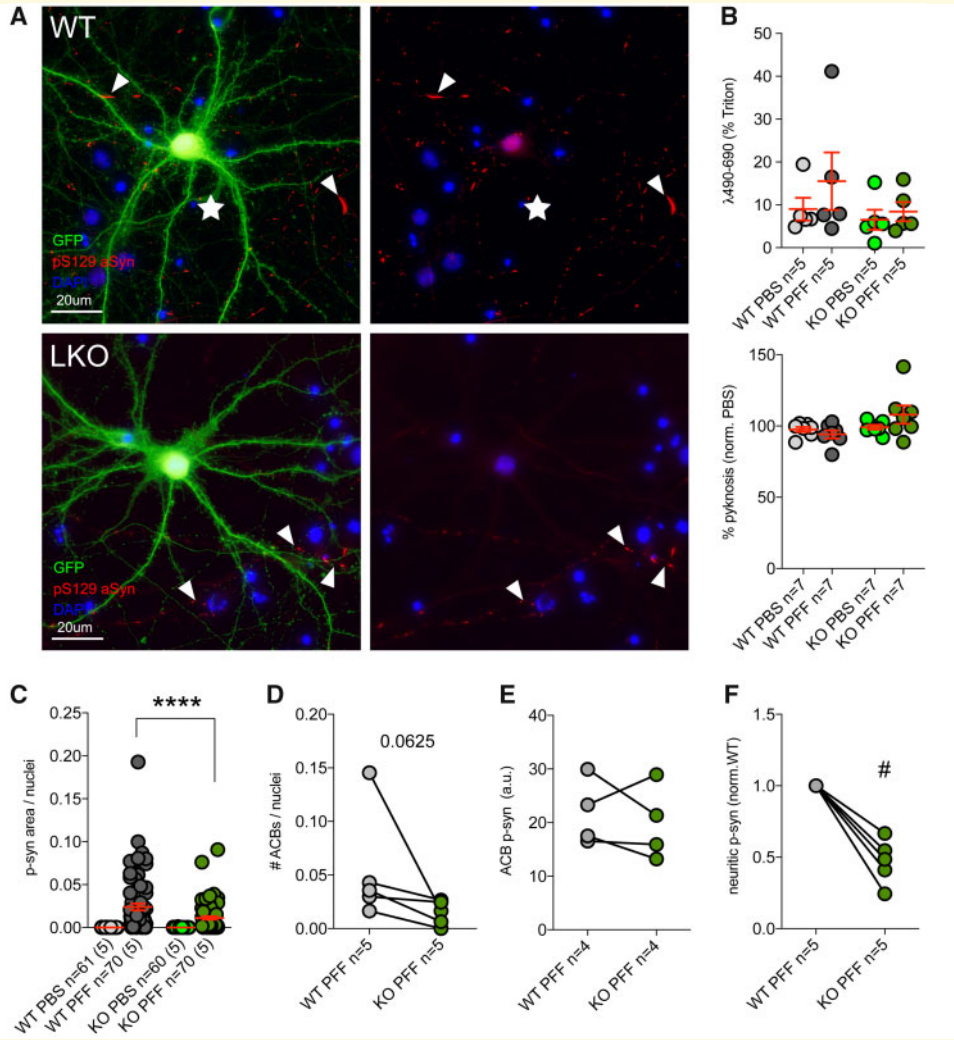

Figure 3 PFF treatment induces pS129 aSyn aggregation without cell death, and genetic knock-out of LRRK2 confers resistance to PFF-induced pS129 aSyn accumulation. (**A**) Representative example (left) immunofluorescent micrograph of GFP expressing (anti-GFP; green) WT and LKO cortical neurons at div17, 10 days following application of PFF. Cultures also stained for nuclei (DAPI; blue) and pS129 aSyn (red). Typical PFF-treated pS129 aSyn staining is observed throughout the image field of WT neurons (closed arrowheads) and within the axon of the GFP-closed cell (closed star). Less signal and fewer aggregates are observed in LKO cultures. (**B**) LDH toxicity assay shows no difference between PBS- and PFF-treated neurons (relative to positive control; 100% cell death by Triton X treatment) and no difference between WT and LKO cultures (one-way RM-ANOVA; $F(1.3,5.0) = 1.8$; $P = 0.25$, $n = 5$ cultures). Pyknotic nuclei counts show no difference between PBS- and PFF-treated neurons (relative to PBS), and no difference between WT and LKO cultures (one-way RM-ANOVA; $F(1.14,6.8) = 3.0$; $P = 0.13$, $n = 7$ cultures). (**C**) Quantification of pS129 aSyn signals [relative to the average number of cells in each culture (DAPI); n=image field and (culture)]; PFF treatment-induced pS129 aSyn signal area is significantly greater in WT than LKO cultures (one-way ANOVA; $F(3,257) = 1.8$; $P = 0.0001$; ****WT PFF versus LKO PFF $P = 0.0001$ by Holm-Sidak *post hoc*). (**D**) Occasional cell soma contains pS129 aSyn aggregates (ACBs; 2–15%, $n = 5$ cultures) in WT cultures, and there is a strong trend towards a smaller percentage of ACB in paired LKO cultures. (**E**) pS129 aSyn signal intensity is not different within ACBs of paired WT and LKO cultures ($n = 4$ cultures). (**F**) When ACBs are eliminated from image analyses (neuritic p-syn), pS129 aSyn signal is significantly higher in WT than paired LKO cultures (normalized for ease of interpretation, statistical analyses conducted on raw values; #paired two-tailed Student's *T*-test $P = 0.036$, $n = 5$ cultures).

Lysosome and autophagy markers increase with PFF treatment, and levels differ in cultures from LKO and GKI mice

The proteasome and the autophagy-lysosome systems are the two primary degradation mechanisms of the cell, and the latter has been proposed to be the predominant pathway by which aSyn degradation occurs; autophagy-lysosome dysfunction has been implicated in Parkinson's disease, and specifically in the accumulation of aSyn (Desplats *et al.*, 2009). Internalized aSyn is targeted to the lysosome (Lee *et al.*, 2008), and lysosomal failure increases aSyn accumulation (Desplats *et al.*, 2009). To

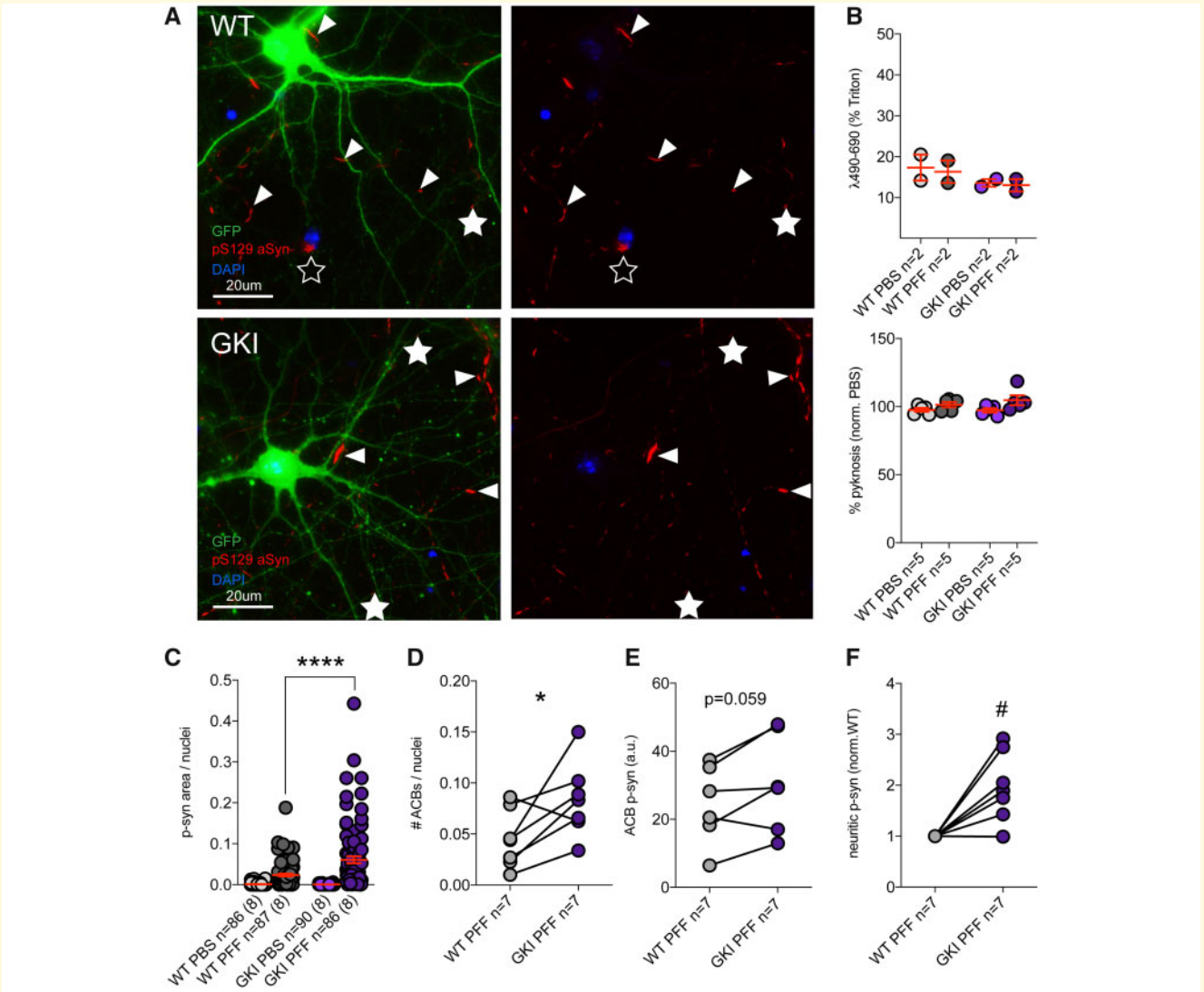

Figure 4 The LRRK2 G2019S point mutation increases susceptibility to PFF-induced pS129 aSyn accumulation in cultures from knock-in mice. (**A**) Representative example (left) immunofluorescent micrograph of GFP expressing (anti-GFP; green) WT and LRRK2 GKI cortical neurons at div17, 10 days following application of PFF. Cultures also stained for nuclei (DAPI; blue) and pS129 aSyn (red). Typical PFF-treated pS129 aSyn staining is observed throughout the image field of WT neurons (closed arrowheads) and within the axon of a GFP-closed cell (closed star, apical point). An pS129 aSyn containing cell body is apparent in this image field (open star). Increased signal and more numerous aggregates are observed in GKI cultures. (**B**) LDH toxicity assay shows no difference between PBS- and PFF-treated neurons (relative to positive control; 100% cell death by Triton X treatment) and no difference between WT and GKI cultures (one-way RM-ANOVA; $F(1,1) = 4$; $P = 0.3$, $n = 2$ cultures). Pyknotic nuclei counts show no difference between PBS- and PFF-treated neurons (relative to PBS), and no difference between WT and GKI cultures (one-way RM-ANOVA; $F(3,16) = 2.3$; $P = 0.12$, $n = 5$ cultures). (**C**) Quantification of pS129 aSyn signals [relative to the average number of cells in each culture (DAPI); n = image field and (culture)]; PFF treatment-induced pS129 aSyn signal area is significantly greater in WT than GKI cultures [one-way ANOVA; $F(3,345) = 38.21$; $P = 0.0001$; ****WT PFF versus LKO PFF $P = 0.0001$ by Holm-Sidak *post hoc*, n = image field and (culture)]. (**D**) Occasional cell soma contain pS129 aSyn aggregates (ACBs; 1–9%) in WT cultures, and there is a significantly higher percentage of ACB in paired GKI cultures (*paired Student's *T*-test $P = 0.041$, $n = 7$ cultures). (**E**) pS129 aSyn signal intensity is trending to being increased within ACBs of paired WT and GKI cultures ($n = 7$ cultures). (**F**) When ACBs are eliminated from image analyses (neuritic p-syn), pS129 aSyn signal is significantly higher in GKI than paired WT cultures (normalized for visualization, statistical analyses conducted on raw values; #paired two-tailed Student's *T*-test $P = 0.031$, $n = 7$ cultures).

examine potential genetic effects of LRRK2 in autophagy and lysosomal function that may contribute to neuronal sensitivity to PFF-induced pathology, staining of the canonical lysosomal marker LAMP1, and p62, an adaptor protein that recruits autophagy machinery to protein aggregates, including those produced by PFFs (Tanik *et al.*, 2013; Karampetsou *et al.*, 2017; Hoffmann *et al.*, 2019) was conducted.

In WT cells (from either LKO or GKI breeds) treated with PBS, LAMP1 signal was diffusely punctate, throughout the soma, and apparent within proximal dendrites (Fig. 5A). Contrastingly, in PFF-treated cells LAMP1 signal became more reticular (Fig. 5A), and signal area increased within image fields (Fig. 5B). A similar basal signal and response to PFF treatment were observed in GKI neurons (Fig. 5B); however, LKO cells had significantly higher LAMP1 signal at base (PBS control), to the same degree as the increased produced by PFF treatment in WT and GKI cells, which did not increase following PFF treatment. Quantification of LAMP1 signal intensity only within ACBs (containing pS129 aSyn aggregates) showed a similar level of LAMP1 staining in WT, LKO and GKI (Fig. 5A and C) and there was no significant difference in co-localization of pS129 aSyn and LAMP1 (Fig. 5A and D).

The pattern of p62 staining in WT, LKO and GKI cells was similar in PBS-treated cultures; being diffusely punctate throughout the soma and apparent within proximal dendrites (Fig. 5A). Although the pattern of p62 signal was similar in all genotypes, and levels were similar between LKO and WT cells, the field signal area was significantly greater in PBS-treated neurons of GKI cultures relative to WT (Fig. 5E). In cells treated with PFF, p62 signal increased significantly in all genotypes (Fig. 5E). Although p62 levels increase with PFF treatment, quantification of p62 signal intensity within ACBs (containing pS129 aSyn aggregates) showed a similar level of p62 in WT, LKO, and GKI (Fig. 5A and F). In ACBs, p62 decorated somatic pS129 aSyn aggregates to a high degree, as evidenced by a ~60% co-localization overlap (Pearson's *R* coefficient), but there was no significant difference between genotypes (Fig. 5A and G).

Discussion

As far as we are aware, the results here are the first demonstration of enhanced susceptibility to PFF-induced aSyn aggregation in neurons from G2019S germ-line knock-in mice. This is in agreement with similarly enhanced aggregation observed in cultures from LRRK2 G2019S overexpressing mice (Volpicelli-Daley *et al.*, 2016; Henderson *et al.*, 2018; Bieri *et al.*, 2019). LRRK2 has many functions in varied cell types throughout the body; glia and other cells have been implicated in the passage of aSyn and LRRK2 function. However, any differences in induced synucleinopathy between genotypes here must be purely neuronal, as we see no glia in our cultures (by Iba1 and GFAP staining, signal was entirely blank, data not shown). Most phosphorylated synuclein staining was within axonal processes, which is consistent with pathological processes beginning at the site of endogenous synuclein function (Sulzer and Edwards, 2019) and staining at axon terminals in untreated neurons (Fig. 1). The pS129 staining in this paradigm is reflective of modifications on endogenous synuclein and does not occur in synuclein knock-out mouse neurons. Differential sensitivity to PFF treatments might, therefore, be engendered by differing levels of synuclein; however, we found no difference in synuclein protein levels by semi-quantitative western blot of knock-out or knock-in cortex (Supplementary Fig. 2).

It is interesting to note that studies using BAC G2019S transgenic mouse hippocampal cultures report only an ~25% increase in pS129 aggregates, relative to littermate controls (Volpicelli-Daley *et al.*, 2016; Henderson *et al.*, 2018; Bieri *et al.*, 2019), in contrast to the ~2-fold increase we observed here. This may reflect technical differences in the preparation and the amount of aggregation induced in controls, and potential ceiling effects i.e. the majority of pS129 signal reported here is neuritic, having formed within axons, and only a small percentage (~5%) of neurons exhibits somatic aggregation in control or mutant cultures. This is much lower than values reported in other studies, e.g. 15–30% in hippocampal cells (Froula *et al.*, 2018). In support of this argument, although there was a trend towards decreased numbers of aggregate-containing ACB in knock-out cultures, and a significant increase in the percentage of cell bodies containing aggregates in knock-in cultures, the percentages of affected cell bodies are very low and the amount of pSyn within affected cell bodies of all genotypes was similar. This highlights that most vulnerability and protection observed here is within the neuropil and argues that once a cell has reached the point where somatic aggregation is occurring, a threshold would appear to have been reached, after which aggregation is equally bad, irrespective LRRK2.

The low percentage of cell bodies affected and the large increase in pSyn aggregation in mutants could also be a reflection of the type of neurons in culture (e.g. hippocampal versus cortical neurons), or the presence of drug vectors in all conditions in other studies (e.g. DMSO) which is potentially stressful. Alternatively, the much greater increase in pS129 aggregation may relate to differences in LRRK2 activity in germ-line knock-in neurons, relative to BAC transgenics. We found knock-in cortical neurons had much more pronounced synaptic phenotypes than those from ~3× WT LRRK2 overexpressing BAC mice (Beccano-Kelly *et al.*, 2014). In support of this, a very recent study demonstrated that LRRK2 G2019S human iPSC-derived neurons exhibit ~2-fold more pS129 aSyn aggregation after 3 weeks, than otherwise isogenic corrected controls (Bieri *et al.*, 2019). We found germ-line silencing of LRRK2 reduced sensitivity to PFF-induced pS129 aSyn aggregation, a result also recently demonstrated in other LKO scenarios, including human neurons (Bieri *et al.*, 2019). These findings, in concert with those that show LRRK2 ASO silencing (Zhao *et al.*, 2017) and LRRK2 kinase inhibition (Volpicelli-Daley *et al.*, 2016) are protective against aSyn inclusion formation, support the argument that LRRK2

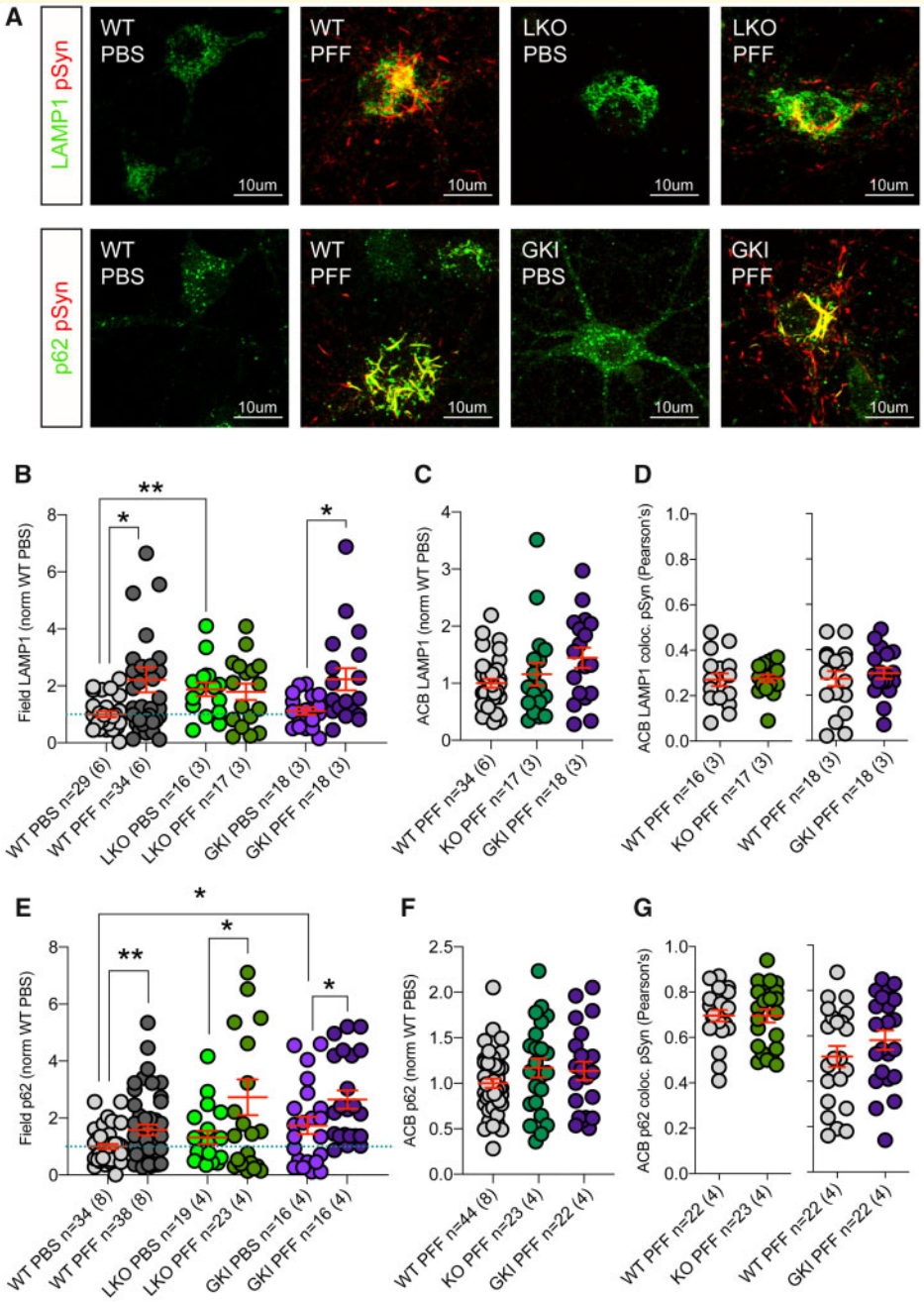

Figure 5 Lysosome and autophagy marker signals increase with PFF treatment, and basal levels are altered in LKO and GKI neurons. (**A**) Representative example (left) confocal immunofluorescent micrographs of LAMP1 or p62 (green) and pS129 aSyn (red) staining in WT, LKO and GKI cortical neurons treated with PBS or PFF. (**B**) Quantification of LAMP1 signal in PFF-treated cultures, relative to PBS within culture. LAMP1 signals increase significantly in WT cultures treated with PFF [Welch's ANOVA; $W(5,50.27) = 5.42$; $P = 0.0005$; *WT PBS versus WT PFF $P = 0.011$ Welch's *post hoc*, n = image field and (culture)]. LAMP1 signal is also significantly increased in GKI cultures with PFF treatment [*GKI PBS versus GKI PFF $P = 0.013$, Welch's *post hoc* n = image field and (culture)]. LAMP1 signal is not increased by PFF treatment, but basal LAMP1 signal is significantly greater in LKO cultures [*WT PBS versus LKO PBS $P = 0.003$ by Welch's *post hoc*, n = image field and (culture)]. (**C**) LAMP1 signal intensity within ACBs is similar in WT, LKO and GKI PFF-treated cultures [Welch's ANOVA; $W(2,28.4) = 2.6$; $P = 0.09$, n = image field and (culture)]. (**D**) Assessment of LAMP1 and pS129 aSyn co-localization (Pearson's R coefficient) within ACBs shows weak co-localization and no difference in LKO or GKI neurons with WT controls [n=image field and (culture)]. (**E**) Quantification of p62 signal in PFF-treated cultures, relative to PBS WT within culture. p62 signals increase significantly in WT, LKO and GKI cultures treated with PFF [Welch's ANOVA; $W(5,59.9) = 7.2$; $P = 0.0001$; **WT PBS versus WT PFF $P = 0.007$, *LKO PBS versus LKO PFF $P = 0.044$, *GKI PBS versus GKI PFF $P = 0.046$, Welch's *post hoc*, n = image field and (culture)]. Basal p62 signal is significantly greater in GKI cultures [*WT PBS versus GKI PBS $P = 0.028$, Welch's *post hoc*, n = image field and (culture)]. (**F**) p62 signal intensity within ACBs is similar in WT, LKO and GKI PFF-treated cultures [Welch's ANOVA; $W(2,39.4) = 1.5$; $P = 0.24$, n = image field and (culture)]. (**G**) Assessment of p62 and pS129 aSyn co-localization (Pearson's R coefficient) within ACBs shows a high degree of co-localization, but no difference between LKO or GKI neurons, compared with WT controls [n = image field and (culture)].

targeting may be beneficial against synucleinopathy. We found no difference in the level of LRRK2 protein in GKI cortex (Supplementary Fig. 2), but it is noteworthy that LRRK2 kinase treatment can dramatically reduce levels of LRRK2, depending on treatment strategy and the reduction in LRRK2 levels may contribute in inhibitor studies elsewhere, regardless of activity *per se*.

As pS129 aSyn aggregates are insoluble, and it is possible that aggregates could be where axons were, which since degenerated, as many were associated with blebbed axonal processes. However, we observed no evidence of PFF-induced cell death over this timeframe, and we did not observe an affected cell body-like aggregate without an associated nucleus, suggesting the vast majority of pS129 aggregates are (or were) within axons. Furthermore, we observed axonal aggregates and fragmented axons within otherwise perfectly healthy-looking neurons. We did not observe pS129 aggregation after seeding with monomeric synuclein, suggesting oligomeric forms are necessary for conversion of endogenous aSyn to pathogenic forms. That said, others have observed aggregation after monomeric treatment of more mature neurons (Hassink *et al.*, 2018), and future studies may determine whether LKO and knock-in cells are differentially affected by monomer-induced aggregation at more mature *in vitro* stages.

LAMP1 levels significantly increased upon PFF treatment throughout the neuropil in WT (and GKI) cultures, but LAMP1 in neuropil was not associated with pSyn aggregates. Furthermore, in cell bodies that did contain large aggregates (ACBs), LAMP1 levels were not increased, and co-localization between pSyn and LAMP1 was not higher than expected for a diffuse somatic marker such as LAMP1 (~25–30% by Pearson's *R* coefficient). Levels of the autophagy adaptor protein p62 similarly increased throughout the neuropil in all cultures, but not within aggregate-containing ACB. However, in contrast to LAMP1, p62 was partially localized with pSyn aggregates in the neuropil, and closely decorated somatic aggregates (~70% coefficient).

While the data here do not provide evidence for causal mechanistic relationships, there are two correlates with genetic protection and vulnerability, respectively, LAMP1 (knock-out cells) and p62 signals being increased. A role for LRRK2 in lysosomal clearance was demonstrated in LKO mice, which exhibit accumulation of enlarged secondary lysosomes in peripheral tissues (Tong *et al.*, 2010; Herzig *et al.*, 2011). Since, under lysosomal overload stress, Rab7L1/Rab29 has been proposed to recruit activated LRRK2 to lysosomal membranes, where phosphorylation of Rab8 and Rab10 promotes stabilization and secretion, respectively (Eguchi *et al.*, 2018). A basal increase in LAMP1 staining in knock-out cells may mean they have more, or more active, lysosomal machinery primed to deal with aSyn degradation within the lysosome. This may explain why LAMP1 signals do not co-localize with pSyn aggregates. LAMP1 signals were not increased in LRRK2 knock-in cells, in agreement with data from LRRK2 G2019S patients (Orenstein *et al.*, 2013). The autophagy marker p62, which transports ubiquitin conjugates to autophagosomes for degradation, has been shown to physically interact with LRRK2 (Park *et al.*, 2016), and may be a LRRK2 phosphorylation substrate (Kalogeropulou *et al.*, 2018). During this process, p62 is constitutively degraded in autophagosomes (Johansen and Lamark, 2011). Thus an increase in p62 signal at base in LRRK2 knock-in mouse cultures suggests the autophagy system is stalling/already under stress. As autophagy is one of the major degradation pathways for aSyn, basal impairment here may well contribute to increased sensitivity of LRRK2 mutant neurons to PFF-induced pSyn aggregation. How basal levels of p62 or LAMP1 might translate to reports of *in vivo* and *in vitro* vulnerability to PFF-induced aggregation in G2019S scenarios is unclear; however, we found no evidence for increases in p62 in cortical lysates, and while LAMP1 quantification was not achieved, correlative changes in levels were also not apparent (Supplementary Fig. 2).

In summary, neurons from G2019S germ-line knock-in mice are more sensitive to *in vitro* PFF-induced pSyn conversion, whereas LRRK2 gene-silenced neurons are partially protected. This adds to a growing number of studies that argue LRRK2 silencing, and potentially inhibition, may be a useful therapeutic strategy against synucleinopathy.

Supplementary material

Supplementary material is available at *Brain Communications* online.

Funding

This work was supported by the Michael J Fox Foundation (A.J.M.), Parkinson Canada (A.J.M., M.V.), Canada Excellence in Research Chairs (M.J.F.) and a Canadian Institutes for Health Research doctoral award (S.M.).

Competing interests

The authors report no competing interests.

References

Beccano-Kelly DA, Kuhlmann N, Tatarnikov I, Volta M, Munsie LN, Chou P, et al. Synaptic function is modulated by LRRK2 and glutamate release is increased in cortical neurons of G2019S LRRK2 knock-in mice. Front Cell Neurosci 2014; 8:301.

Beccano-Kelly DA, Volta M, Munsie LN, Paschall SA, Tatarnikov I, Co K, et al. LRRK2 overexpression alters glutamatergic presynaptic

plasticity, striatal dopamine tone, postsynaptic signal transduction, motor activity and memory. Hum Mol Genet 2015; 24: 1336–49.
Bieri G, Brahic M, Bousset L, Couthouis J, Kramer NJ, Ma R, et al. LRRK2 modifies α-syn pathology and spread in mouse models and human neurons. Acta Neuropathol 2019; 137: 961–80.
Brundin P, Melki R. Prying into the Prion Hypothesis for Parkinson's Disease. J Neurosci 2017; 37: 9808–18.
Cresto N, Gardier C, Gubinelli F, Gaillard MC, Liot G, West AB, et al. The unlikely partnership between LRRK2 and α-synuclein in Parkinson's disease. Eur J Neurosci 2019; 49: 339–63.
Daher JP, Abdelmotilib HA, Hu X, Volpicelli-Daley LA, Moehle MS, Fraser KB, et al. Leucine-rich repeat kinase 2 (LRRK2) pharmacological inhibition abates alpha-synuclein gene-induced neurodegeneration. J Biol Chem 2015; 290: 19433–44.
Daher JP, Pletnikova O, Biskup S, Musso A, Gellhaar S, Galter D, et al. Neurodegenerative phenotypes in an A53T alpha-synuclein transgenic mouse model are independent of LRRK2. Hum Mol Genet 2012; 21: 2420–31.
Daher JP, Volpicelli-Daley LA, Blackburn JP, Moehle MS, West AB. Abrogation of alpha-synuclein-mediated dopaminergic neurodegeneration in LRRK2-deficient rats. Proc Natl Acad Sci U S A 2014; 111: 9289–94.
Desplats P, Lee HJ, Bae EJ, Patrick C, Rockenstein E, Crews L, et al. Inclusion formation and neuronal cell death through neuron-to-neuron transmission of alpha-synuclein. Proc Natl Acad Sci U S A 2009; 106: 13010–5.
Eguchi T, Kuwahara T, Sakurai M, Komori T, Fujimoto T, Ito G, et al. LRRK2 and its substrate Rab GTPases are sequentially targeted onto stressed lysosomes and maintain their homeostasis. Proc Natl Acad Sci U S A 2018; 115: E9115–24.
Emmanouilidou E, Minakaki G, Keramioti MV, Xylaki M, Balafas E, Chrysanthou-Piterou M, et al. GABA transmission via ATP-dependent K+ channels regulates α-synuclein secretion in mouse striatum. Brain 2016; 139: 871–90.
Foffani G, Obeso JA. A cortical pathogenic theory of Parkinson's disease. Neuron 2018; 99: 1116–28.
Froula JM, Henderson BW, Gonzalez JC, Vaden JH, Mclean JW, Wu Y, et al. α-Synuclein fibril-induced paradoxical structural and functional defects in hippocampal neurons. Acta Neuropathol Commun 2018; 6: 35.
Fujiwara H, Hasegawa M, Dohmae N, Kawashima A, Masliah E, Goldberg MS, et al. α-synuclein is phosphorylated in synucleinopathy lesions. Nat Cell Biol 2002; 4: 160–4.
Giguère N, Nanni SB, Trudeau LE. On cell loss and selective vulnerability of neuronal populations in Parkinson's disease. Front Neurol 2018; 9: 455.
Goedert M, Spillantini MG, Del Tredici K, Braak H. 100 years of Lewy pathology. Nat Rev Neurol 2013; 9: 13–24.
Hassink GC, Raiss CC, Segers-Nolten IMJ, Van Wezel RJA, Subramaniam V, Le Feber J, et al. Exogenous α-synuclein hinders synaptic communication in cultured cortical primary rat neurons. PLoS One 2018; 13: e0193763.
Henderson MX, Peng C, Trojanowski JQ, Lee V. LRRK2 activity does not dramatically alter α-synuclein pathology in primary neurons. Acta Neuropathol Commun 2018; 6: 45.
Henderson MX, Sengupta M, McGeary I, Zhang B, Olufemi MF, Brown H, et al. LRRK2 inhibition does not impart protection from α-synuclein pathology and neuron death in non-transgenic mice. Acta Neuropathol Commun 2019; 7: 28.
Herzig MC, Bidinosti M, Schweizer T, Hafner T, Stemmelen C, Weiss A, et al. High LRRK2 levels fail to induce or exacerbate neuronal alpha-synucleinopathy in mouse brain. PLoS One 2012; 7: e36581.
Herzig MC, Kolly C, Persohn E, Theil D, Schweizer T, Hafner T, et al. LRRK2 protein levels are determined by kinase function and are crucial for kidney and lung homeostasis in mice. Hum Mol Genet 2011; 20: 4209–23.
Hoffmann AC, Minakaki G, Menges S, Salvi R, Savitskiy S, Kazman A, et al. Extracellular aggregated alpha synuclein primarily triggers lysosomal dysfunction in neural cells prevented by trehalose. Sci Rep 2019; 9: 1–18.
Johansen T, Lamark T. Selective autophagy mediated by autophagic adapter proteins. Autophagy 2011; 7: 279–96.
Kalogeropulou AF, Zhao J, Bolliger MF, Memou A, Narasimha S, Molitor TP, et al. P62/SQSTM1 is a novel leucine-rich repeat kinase 2 (LRRK2) substrate that enhances neuronal toxicity. Biochem J 2018; 475: 1271–93.
Karampetsou M, Ardah MT, Semitekolou M, Polissidis A, Samiotaki M, Kalomoiri M, et al. Phosphorylated exogenous alpha-synuclein fibrils exacerbate pathology and induce neuronal dysfunction in mice. Sci Rep 2017; 7: 1–18.
Kozina E, Sadasivan S, Jiao Y, Dou Y, Ma Z, Tan H, et al. Mutant LRRK2 mediates peripheral and central immune responses leading to neurodegeneration in vivo. Brain 2018; 141: 1753–69.
Lee HJ, Patel S, Lee SJ. Intravesicular localization and exocytosis of alpha-synuclein and its aggregates. J Neurosci 2005; 25: 6016–24.
Lee HJ, Suk JE, Bae EJ, Lee JH, Paik SR, Lee SJ. Assembly-dependent endocytosis and clearance of extracellular alpha-synuclein. Int J Biochem Cell Biol 2008; 40: 1835–49.
Lin X, Parisiadou L, Gu XL, Wang L, Shim H, Sun L, et al. Leucine-rich repeat kinase 2 regulates the progression of neuropathology induced by Parkinson's-disease-related mutant alpha-synuclein. Neuron 2009; 64: 807–27.
Luk KC, Kehm V, Carroll J, Zhang B, O'Brien P, Trojanowski JQ, et al. Pathological alpha-synuclein transmission initiates Parkinson-like neurodegeneration in nontransgenic mice. Science 2012a; 338: 949–53.
Luk KC, Kehm VM, Zhang B, O'Brien P, Trojanowski JQ, Lee VM. Intracerebral inoculation of pathological alpha-synuclein initiates a rapidly progressive neurodegenerative alpha-synucleinopathy in mice. J Exp Med 2012b; 209: 975–86.
Luk KC, Song C, O'Brien P, Stieber A, Branch JR, Brunden KR, et al. Exogenous alpha-synuclein fibrils seed the formation of Lewy body-like intracellular inclusions in cultured cells. Proc Natl Acad Sci U S A 2009; 106: 20051–6.
Munsie LN, Milnerwood AJ, Seibler P, Beccano-Kelly DA, Tatarnikov I, Khinda J, et al. Retromer-dependent neurotransmitter receptor trafficking to synapses is altered by the Parkinson's disease VPS35 mutation p.D620N. Hum Mol Genet 2015; 24: 1691–703.
Murphy DD, Rueter SM, Trojanowski JQ, Lee M-Y. Synucleins Are Developmentally Expressed, and α-Synuclein Regulates the Size of the Presynaptic Vesicular Pool in Primary Hippocampal Neurons. J Neurosci 2000; 20: 3214–20.
Orenstein SJ, Kuo SH, Tasset I, Arias E, Koga H, Fernandez-Carasa I, et al. Interplay of LRRK2 with chaperone-mediated autophagy. Nat Neurosci 2013; 16: 394–406.
Paillusson S, Clairembault T, Biraud M, Neunlist M, Derkinderen P. Activity-dependent secretion of alpha-synuclein by enteric neurons. J Neurochem 2013; 125: 512–7.
Park S, Han S, Choi I, Kim B, Park SP, Joe EH, et al. Interplay between leucine-rich repeat kinase 2 (LRRK2) and p62/SQSTM-1 in selective autophagy. PLoS One 2016; 11: 1–14.
Paumier KL, Luk KC, Manfredsson FP, Kanaan NM, Lipton JW, Collier TJ, et al. Intrastriatal injection of pre-formed mouse alpha-synuclein fibrils into rats triggers alpha-synuclein pathology and bilateral nigrostriatal degeneration. Neurobiol Dis 2015; 82: 185–99.
Puccini JM, Marker DF, Fitzgerald T, Barbieri J, Kim CS, Miller-Rhodes P, et al. Leucine-Rich Repeat Kinase 2 Modulates Neuroinflammation and Neurotoxicity in Models of Human Immunodeficiency Virus 1-Associated Neurocognitive Disorders. J Neurosci 2015; 35: 5271–83.
Sulzer D, Edwards RH. The physiological role of α-synuclein and its relationship to Parkinson's Disease. J Neurochem 2019; 150: 475–86.

Surmeier DJ, Obeso JA, Halliday GM. Parkinson's disease is not simply a prion disorder. J Neurosci 2017; 37: 9799–807.

Taguchi K, Watanabe Y, Tsujimura A, Tanaka M. Brain region-dependent differential expression of alpha-synuclein. J Comp Neurol 2016; 524: 1236–58.

Tanik SA, Schultheiss CE, Volpicelli-Daley LA, Brunden KR, Lee VM. Lewy body-like alpha-synuclein aggregates resist degradation and impair macroautophagy. J Biol Chem 2013; 288: 15194–210.

Thévenet J, Gobert R, van Huijsduijnen RH, Wiessner C, Sagot YJ. Regulation of LRRK2 expression points to a functional role in human monocyte maturation. PLoS One 2011; 6: e21519.

Tong Y, Yamaguchi H, Giaime E, Boyle S, Kopan R, Kelleher RJ 3rd, et al. Loss of leucine-rich repeat kinase 2 causes impairment of protein degradation pathways, accumulation of alpha-synuclein, and apoptotic cell death in aged mice. Proc Natl Acad Sci U S A 2010; 107: 9879–84.

Volpicelli-Daley LA, Abdelmotilib H, Liu Z, Stoyka L, Daher JP, Milnerwood AJ, et al. G2019S-LRRK2 expression augments alpha-synuclein sequestration into inclusions in neurons. J Neurosci 2016; 36: 7415–27.

Volpicelli-Daley LA, Gamble KL, Schultheiss CE, Riddle DM, West AB, Lee VM. Formation of alpha-synuclein Lewy neurite-like aggregates in axons impedes the transport of distinct endosomes. Mol Biol Cell 2014a; 25: 4010–23.

Volpicelli-Daley LA, Luk KC, Lee VM. Addition of exogenous alpha-synuclein preformed fibrils to primary neuronal cultures to seed recruitment of endogenous alpha-synuclein to Lewy body and Lewy neurite-like aggregates. Nat Protoc 2014b; 9: 2135–46.

Volpicelli-Daley LA, Luk KC, Patel TP, Tanik SA, Riddle DM, Stieber A, et al. Exogenous alpha-synuclein fibrils induce Lewy body pathology leading to synaptic dysfunction and neuron death. Neuron 2011; 72: 57–71.

Volta M, Beccano-Kelly DA, Paschall SA, Cataldi S, MacIsaac SE, Kuhlmann N, et al. Initial elevations in glutamate and dopamine neurotransmission decline with age, as does exploratory behavior, in LRRK2 G2019S knock-in mice. Elife 2017; 6: e28377.

Volta M, Milnerwood AJ, Farrer MJ. Insights from late-onset familial parkinsonism on the pathogenesis of idiopathic Parkinson's disease. Lancet Neurol 2015; 14: 1054–64.

Zhao HT, John N, Delic V, Ikeda-Lee K, Kim A, Weihofen A, et al. LRRK2 antisense oligonucleotides ameliorate α-synuclein inclusion formation in a Parkinson's disease mouse model. Mol. Ther. Nucleic Acids 2017; 8: 508–19.